d-Ti$_3$C$_2$ /MoS$_2$ composite for Efficient Electrocatalytic Hydrogen Evolution

I. Ashraf , S. Ahmad , M. Iqbal[*]

Department of Chemistry, School of Natural Sciences (SNS), National University of Sciences and Technology (NUST),
Islamabad, 44000, Pakistan.
*Corresponding author address: mudassir.iqbal@sns.nust.edu.pk

Abstract

MXenes, a two-dimensional material, is an emerging research area. Herein, a d-Ti$_3$C$_2$ MXene was combined with MoS$_2$ nanoballs to achieve better electrocatalytic performance for hydrogen evolution reaction (HER). The synthesized d-Ti$_3$C$_2$/MoS$_2$ composite showed outstanding kinetic metrics for electrocatalytic HER, exhibiting a low overpotential of 45 mV at a current density of 10 mA/cm^2 compared to d-Ti$_3$C$_2$ MXene (180 mV) and MoS$_2$ nanoballs (140 mV). Long-term stability was verified for 24 h with a negligible loss in current density. The high electrocatalytic performance of d-Ti$_3$C$_2$/MoS$_2$ composite is believed to be originated from a synergistic effect between d-Ti$_3$C$_2$ MXene and MoS$_2$ nanoballs as well as high metallic conductivity of d-Ti$_3$C$_2$ MXene. It was concluded that the proposed synthesized composite provides insights for fabricating new cost-effective non-noble metal-based electrocatalysts with efficient water-splitting.

Keywords: MXenes, d-Ti3C2 /MoS2 composite, electrocatalytic performance, cost-effective, water-splitting

1.   INTRODUCTION

Hydrogen energy is an efficient energy source. The most common way to obtain hydrogen is water electrolysis, which is abundant in nature. Noble metals such as Platinum (Pt) have shown good electrocatalytic activity in HER [1]. But its large-scale application is limited due to its high price [2, 3]. To find an inexpensive and highly active HER electrocatalyst has become an urgent need. Hydrogen (H$_2$) production, which is directly generated by utilizing semiconducting electrocatalysts, could provide an environmentally friendly approach to solving global issues. Transition metal sulfides such as NiS, MoS$_2$, WS$_2$, and CoS$_2$ have attracted considerable attention as an electrocatalyst for HER because of their low cost and excellent electrocatalytic properties [4-6]. MoS$_2$ in bulk form is a poor catalyst, whereas MoS$_2$ in nano form is a suitable electrocatalyst [7]. Many efforts have been made to synthesize composites of MoS$_2$ to attain excellent HER activity [8, 9]. There are many ways to improve the catalytic activity of MoS$_2$ such as Co, Ni, and Fe were added previously to enhance intrinsic activity [9-11], as well as highly conducting materials can be added to improve electrical contact, including carbon nanotubes (CNTs), graphene oxide, carbon nanofibers, MXene [12-16], etc.

MXenes are two-dimensional (2D) metal carbides, nitrides, or carbonitrides derived from their MAX phase precursor, by selecting the removal of A. The general formula for MXene is M$_{n+1}$X$_n$T$_x$. Where M represents transition metal, X represents C/N and T$_x$ represents surface terminations such as =O, -OH, F [17]. MXenes have attracted researchers because of their versatile properties, such as electrical conductivity, rate capability, surface area, outstanding internal resistance etc. [18]. They are explored for various applications such as environmental, energy, catalysis, electronics, biomedical, and many others [19, 20]. Due to enhanced surface area, it provides multiple reactive sites for electrocatalytic activity; as a result, the charge transfer rate is increased. Among MXenes, many efforts have been made for Ti$_3$C$_2$ MXene, as it is considered a potential candidate for cocatalysts [21]. It has been noted from previously reported literature that Ti$_3$C$_2$ MXene has the potential to replace Pt in electrocatalytic reactions [22]. The charge transfer between Ti$_3$C$_2$ MXene to the active sites is more outstanding than most semiconducting catalysts. Moreover, the H adsorption energy on the surface of MXene is close to 0, thus making it the best among noble metal-free catalysts for application in HER [23]. Water splitting is an essential reaction in fuel cells, solar energy and catalysis. Water splitting for hydrogen production can be done using different methods, including electrolysis, thermolysis, photoelectrolysis, solar light splitting etc.

In the present work, we synthesized d-Ti$_3$C$_2$/MoS$_2$ composite by hydrothermal approach. MoS$_2$ was newly synthesized by a hydrothermal approach that has not been reported yet, whereas d-Ti$_3$C$_2$ MXene was synthesized from its MAX (Ti$_3$SiC$_2$) phase precursor by wet chemical etching. The resulting composite showed outstanding HER activity with 45 mV overpotential and long-term stability and efficient water-splitting. This work can be proved useful to renewably generate hydrogen fuel from water. This is a prospective method to produce environmentally friendly hydrogen fuel.

2. Materials and Methods

2.1. Synthesis of d-Ti$_3$C$_2$ MXene

Ti$_3$C$_2$ MXene was synthesized by one of the reported method [24] by etching of silicon layer from Ti$_3$SiC$_2$ MAX phase precursor using HF as an etching source. At first, the mixture of HF/H$_2$O$_2$ was prepared by the addition of 2.5 mL H$_2$O$_2$ in 22 mL of HF in polypropylene bottle. The solution mixture was stirred in an ice bath to maintain a temperature at 0 ˚C for about 30 minutes. Then 1.5 g of Ti$_3$SiC$_2$ was slowly added, and stirred the mixture for 1.5 h. The polypropylene tube was shifted to a pre-heated oil bath at 40 ˚C for 45 h. This acidic solution was washed with deionized water and ethanol about 5 times to maintain neutral pH using a centrifuge machine. The black color product was obtained and dried in a vacuum oven at 50 ˚C for 24 h. To obtain a delaminated MXene, 1 mL of TMAOH was added to Ti$_3$C$_2$ MXene

(0.5 g) and diluted with 10 mL DI H_2O. The solution was stirred for 24 h at room temperature. The washing was carried out by the same process as discussed above for Ti_3C_2 MXene. The product obtained was dried in a vacuum oven at 50 ˚C for 24 h.

2.2. Synthesis of MoS₂ nanoballs

Ammonium heptamolybedate $(NH_4)_6Mo_7O_{24}.4H_2O$ was added to the deionized (DI) water and was stirred until a uniform suspension was attained. Then, hydrazine hydrate $(N_2H_4.H_2O)$ was added to the solution mixture followed by magnetic stirring for half hour. A Sodium bisulfide (Na_2S) was added to the mixture as a sulfur source. After uniform mixing 10 mL of nitic acid (HNO_3) was added and stirred for 1 hour. After formation of homogeneous mixture, this solution was transferred to the Teflon-lined steel autoclave and shifted to heating oven for 12 h at 160 ˚C. The solution was then cooled down at room temperature in order to perform washing by using DI H_2O and ethanol. The sample was washed for about 5 cycles until neutral pH was attained at 5000 rpm. After washing, the sample was dried in a vacuum oven at 60 ℃ for 12 h.

2.3. Synthesis of d-Ti₃C₂/MoS₂

Primarily, 0.25 mmol of d-Ti_3C_2 MXene was stirred in 20 mL DI water for 10 min to form a good suspension. Similarly, 0.25 mmol of MoS_2 nanoballs were stirred in 20 ml DI water for 20 min. Then the mixture of d-Ti_3C_2 MXene was transferred to the MoS_2 nanoballs solution, and the resulting mixture was sonicated for 10 minutes. This suspension was transferred to a Teflon-lined steel autoclave at 120 ˚C for 12 h. The mixture was cooled at room temperature and then washed with DI water at 3500 rpm via centrifugation for 3 cycles. After washing, the black-colored sample was dried in a vacuum oven at 60 ˚C for 24 h. The scheme for synthesis of d-Ti_3C_2/MoS_2 is shown in **Figure 1**.
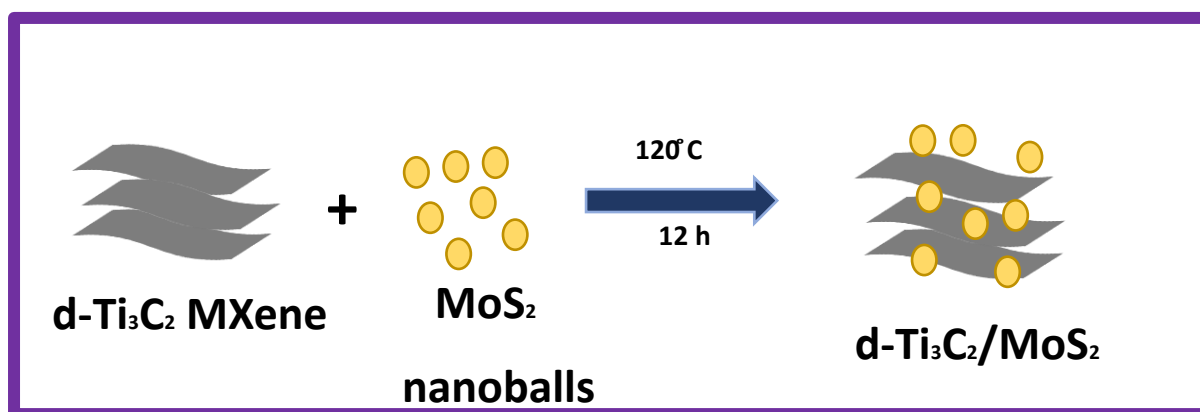
Figure 1. Scheme for synthesis of d-Ti_3C_2/MoS_2

2.4. Material Characterization

XRD for all the samples was measured by Malvern Panalytical Empyrean Raman spectroscopy, carried out by URaman-532 TEC-Ci. The structure morphology was confirmed by scanning electron microscopy (SEM) using VEGA3 TESCAN and Energy-dispersive X-ray spectroscopy (EDX) by Oxford Instrument X-act. X-ray Photoelectron Spectroscopy (XPS) was carried out by Thermo K Alpha with a monochromatic beam of Aluminum K Alpha X Rays.

2.5. Electrochemical measurement

The electrochemical tests for HER were done using Gamry Instruments equipped with three electrode systems. Nickel foam was used as a working electrode with active material. The loading amount of active material was 2 mg. The working electrode was prepared by adding 2 drops of Nafion binder to the mixture of active material and ethanol. The slurry was drop cast onto Ni foam and dried in a vacuum oven for 12 h at 50 ˚C. Pt wire was used as a counter electrode, while Ag/AgCl as a reference electrode. IM KOH solution was used to analyze catalytic activities at $10\ mVs^{-1}$. Similarly, for further calculation Reversible hydrogen electrode (RHE) was used which was achieved by using the following Nernst Equation:

$$E_{RHE} = E_{Ag/AgCl} + 0.059pH + 0.1976.$$

Electrochemical Impedance Spectroscopy (EIS) was accomplished in the frequency range of 0.1 Hz-10 kHz, by providing a 10 mV alternating voltage amplitude. Furthermore, chronoamperometry measurement was used to check the stability of as prepared hybrid nanostructure.

3. RESULTS AND DISCUSSIONS

3.1. X-ray diffraction (XRD) analysis

XRD validated the crystalline structure of all prepared electrodes. **Figure 2** shows XRD pattern of Ti_3SiC_2, d-Ti_3C_2 MXene, MoS_2 nanoballs, d-Ti_3C_2/MoS_2. The diffraction peaks appeared at 9.5˚, 19˚, 29˚ and 39˚ corresponding to (002), (004), (006), and (008) lanes of Ti_3SiC_2, respectively. It is seen that the crystallinity of MAX phase is decreased after treatment with HF/H_2O_2 mixture. In the XRD pattern of d-Ti_3C_2 MXene, the peak at 9.5 ˚ decreased and broadened to a

lower angle due to larger d-spacing. The most intense and sharp peak at about 39° vanishes which indicates that Si layer is successfully removed [281]. In the XRD pattern of MoS_2 nanoballs, the high intense diffraction peak of (002) plane indicates good crystallinity. Similarly, the peaks at the (100) and (110) planes demonstrate the existence of MoS_2 nanoballs. No signal of the impurity phase was detected, indicating the high purity of MoS_2 nanoballs. Notably, diffraction peaks of $d\text{-}Ti_3C_2$ and MoS_2 nanoballs are observed in the XRD pattern of $d\text{-}Ti_3C_2/MoS_2$, which indicates successful synthesis. The c-lattice parameter (c-lp) calculated for $d\text{-}Ti_3C_2$ MXene was 25 Å, whereas for $d\text{-}Ti_3C_2/MoS_2$ 27 Å. The increase in the c-lp of d- $d\text{-}Ti_3C_2/MoS_2$ indicates that this nanocomposite has attained greater interlayer distance because of the successful incorporation of MoS_2 nanoballs in $d\text{-}Ti_3C_2$ MXene.
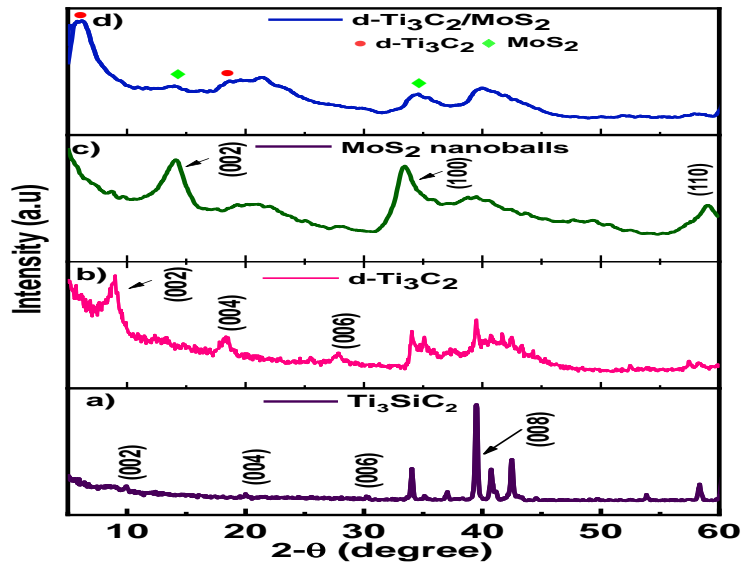
Figure 2. XRD pattern of a) Ti_3SiC_2, b) $d\text{-}Ti_3C_2$, c) MoS_2 nanoballs, d) $d\text{-}Ti_3C_2/MoS_2$

3.2. X-ray photoelectron (XPS) spectroscopy

Figure 3a shows the X-ray photoelectron (XPS) spectroscopy analysis of $d\text{-}Ti_3C_2/MoS_2$ nanocomposite. From the survey spectra, it can be seen that Ti, C, O, Mo, S, and F elements were detected. In the Ti2p spectrum, three fitting peaks at 454.8, 458.6, and 465.3 eV binding energies correspond to Ti-C and Ti-O bonding as shown in **Figure 3b**. In **Figure 3c** the largest C1s signal (284.8 eV) corresponds to Ti-C bond. In the Mo3d spectrum, the three fitting peaks at 232, 228.6, and 226 eV were assigned to Mo3d3/2, Mo3d5/2, and S2s as represented in **Figure 3d**. The S2p1/2 and S2p3/2 peaks were observed in the S2p spectrum at 162.4 and 161.3 eV shown in **Figure 3e**.
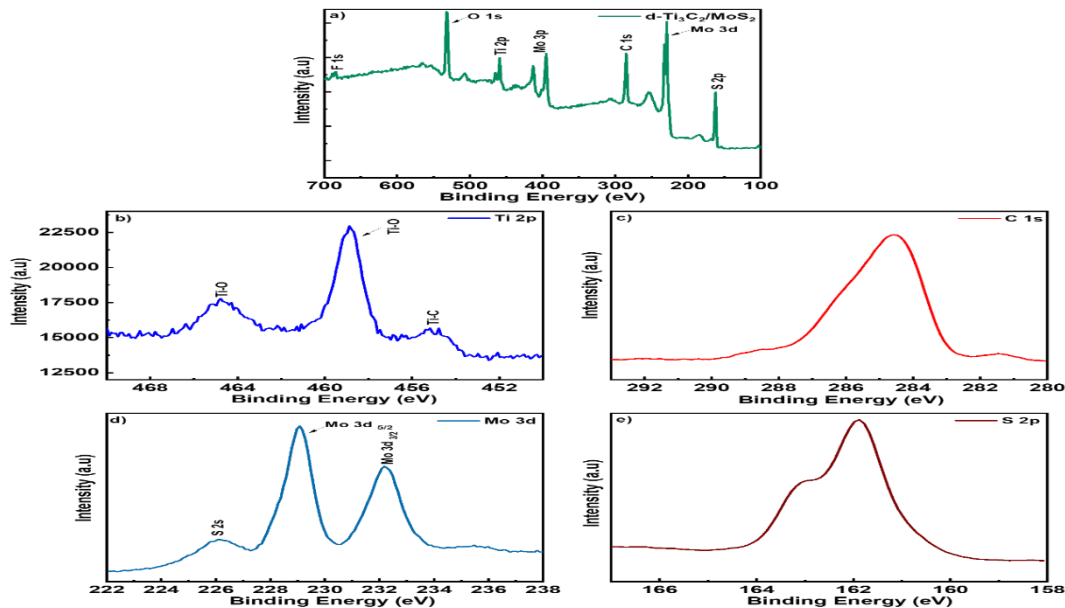
Figure 3a) XPS survey spectra of $d\text{-}Ti_3C_2/MoS_2$,XPS analysis of b) Ti 2p, c) C 1s, d) Mo 3d, e) S 2p

3.3.   Scanning electron microscopy (SEM) and energy-dispersive X-ray spectroscopy (EDX) analysis

SEM analysis was performed to study the morphology and homogeneity of the prepared nanostructures, **Figure 4a-c** shows SEM images of d-Ti$_3$C$_2$ MXene, MoS$_2$ nanoballs, and Ti$_3$C$_2$/MoS$_2$ nanocomposite at 2μm. **Figure 4a** shows the multilayered Ti3C2 MXene at 2μm, indicating that silicon atoms are successfully removed, and an extension of distance between layers occurred. **Figure 4b** shows SEM images of MoS$_2$ nanoballs, which indicates the formation of large-scale, dense, and uniform nanoballs of MoS$_2$ that are interconnected. Similarly, in the SEM image of d-Ti$_3$C$_2$/MoS$_2$ nanocomposite, as shown in **Figure 4c,** Ti$_3$C$_2$ nanosheets and uniform anchoring of MoS$_2$ nanoballs on the MXene layers are observed, which indicates successful synthesis of our nanocomposite. This arrangement increases the composite material's surface area, providing HER multi-catalytic active sites. The EDX spectrum shows the presence of Ti, C, Mo and S elements in the synthesized nanocomposite, as shown in **Figure 4d**. The intense signal of Mo and S indicates that MoS$_2$ nanoballs are successfully incorporated into Ti$_3$C$_2$ MXene nanosheets.
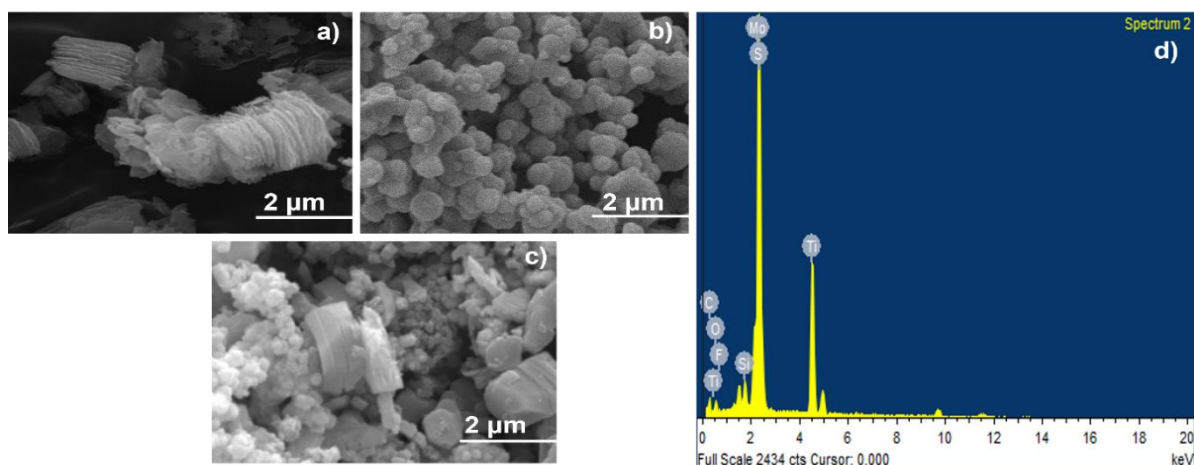
Figure 3. SEM analysis of a) d-Ti$_3$C$_2$, b) MoS$_2$ nanoballs, c) d-Ti$_3$C$_2$/MoS$_2$ d) EDX spectrum d-Ti$_3$C$_2$/MoS$_2$

3.4. Electrochemical measurements

An electrolyte of 1M KOH was used for electrochemical measurements. We studied HER activity to analyze the electrocatalytic performance of Ti3C2 MXene, MoS2 nanoballs, and d-Ti3C2/MoS2 nanocomposite. **Figure 5a** shows comparison polarization curves of d-Ti$_3$C$_2$ MXene, MoS$_2$ nanoballs, and d-Ti$_3$C$_2$/MoS$_2$ nanocomposite for HER. As expected, all samples could efficiently drive H$_2$ evolution under negative bias. d-Ti$_3$C$_2$/MoS$_2$ nanocomposite displays a very low overpotential of 45 mV at 10 mA cm^{-2} current density, while MoS$_2$ nanoballs and d-Ti$_3$C$_2$ MXene showed overpotential of 140 and 180 mV. This enhanced electrochemical performance was attributed to the synergistic effect of d-Ti$_3$C$_2$ and MoS$_2$ nanoballs. Tafel slope is considered to evaluate the HER kinetics information. Based on the results mentioned above, the enhanced HER kinetics of d-Ti$_3$C$_2$/MoS$_2$ results from its improved surface area that was increased from incorporating MoS$_2$ nanoballs on d-Ti$_3$C$_2$ MXene as well as higher intrinsic catalytic activity. The electronic synergy between Ti and Mo metal was proved to be more favorable for HER catalysis, in which one component facilitates the adsorption of H-containing intermediate and the second component completes the reaction by facilitating the migration of the adsorbed H to another site.

The smaller Tafel slope values indicated faster HER kinetics and enhanced HER activity. d-Ti$_3$C$_2$/MoS$_2$ nanocomposite exhibited a low Tafel slope of 75 mV dec^{-1} compared to MoS$_2$ nanoballs (92 mV dec^{-1}) and d-Ti$_3$C$_2$ MXenee (98 mV dec^{-1}) as shown in **Figure 5b**. This outstanding electrochemical performance occurred because of the successful incorporation of MoS$_2$ nanoballs on d-Ti$_3$C$_2$ MXene, which increased the surface area as well as the electrical conductivity of the nanocomposite. **Figure 5c** compares overpotential values for d-Ti$_3$C$_2$ MXene, MoS$_2$ nanoballs, and d-Ti$_3$C$_2$/MoS$_2$ nanocomposite. d-Ti$_3$C$_2$/MoS$_2$ indicates the lowest overpotential of 45 mV, which indicates this material has shown good catalytic activity because of increased surface area. **Figure 5d** shows the catalytic durability curve of d- d-Ti$_3$C$_2$/MoS$_2$ after 1000 cycles. A negligible loss was observed after 1000 cycles which indicates our material was catalytically durable.
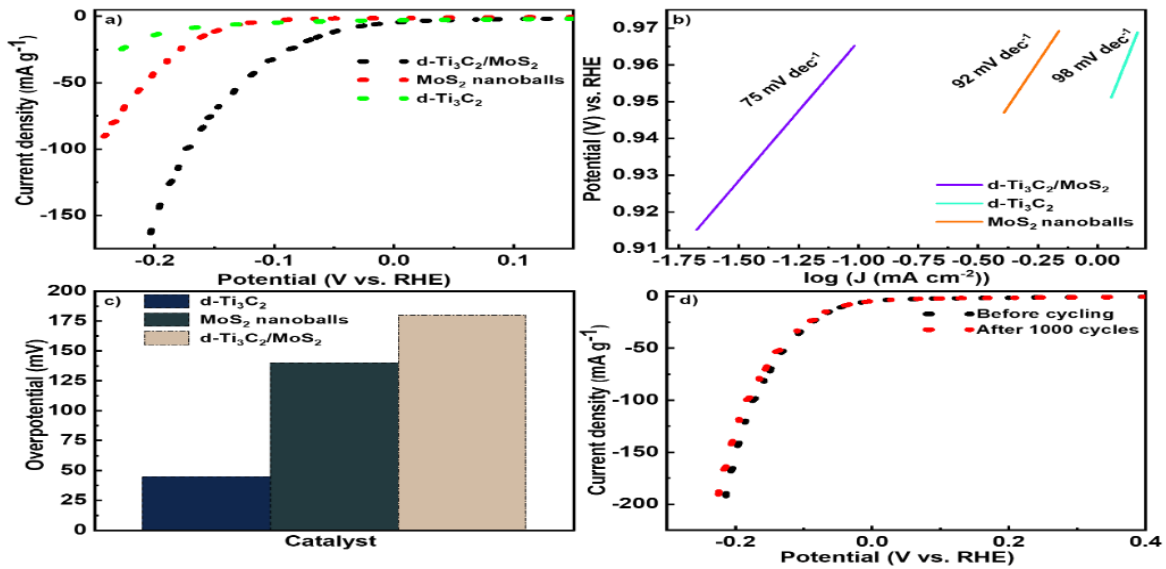
Figure 5. a) LSV, b) Tafel plot, c) Comparison of overpotential of of d-Ti$_3$C$_2$ MXene, MoS$_2$ nanoballs and d-Ti$_3$C$_2$/MoS$_2$ d) Durability curve of d-Ti$_3$C$_2$/MoS$_2$

Figure 6a-c shows the cyclic voltammetry profile of d-Ti$_3$C$_2$ MXene, MoS$_2$ nanoballs and d-Ti$_3$C$_2$/MoS$_2$ nanocomposite in the non-faradic region at different scan rates from 10-50 mV s^{-1}. **Figure 6d** shows a comparison plot of d-Ti$_3$C$_2$ MXene, MoS$_2$ nanoballs, and d-Ti$_3$C$_2$/MoS$_2$ nanocomposite at 10 mV s^{-1}. It was seen that d-Ti$_3$C$_2$/MoS$_2$ shows the highest current density of 7.2 mA, indicating that this material possesses a greater value of double-layer capacitance due to an increase in its area. **Figure 7a** shows the EIS pattern of all synthesized materials. The EIS patterns indicate lower charge transfers resistance of d-Ti$_3$C$_2$/MoS$_2$ among d-Ti$_3$C$_2$ and MoS$_2$ nanoballs. This occurred due to the better conductivity of d-Ti$_3$C$_2$/MoS$_2$, which is related to more active sites and greater charge transfer rate from the electrode to the electrolyte.
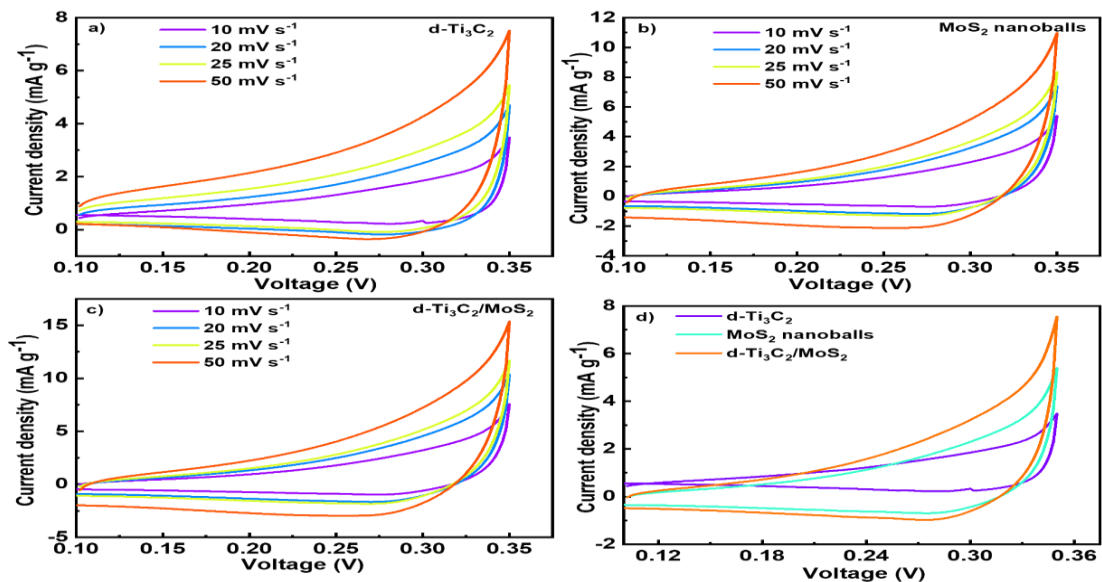
Figure 6. CV profile of a) d-Ti$_3$C$_2$, b) MoS$_2$ nanoballs c) d-Ti$_3$C$_2$/MoS$_2$ d) Comparison CV plot at 10 mV s^{-1}.

Chronoamperometry was carried out to check the stability of d-Ti$_3$C$_2$/MoS$_2$. The test was conducted for 20 h at 10 mV s^{-1} as shown in **Figure 7b**. The result indicates a slight loss after 20 h, which indicates good stability of d-Ti$_3$C$_2$/MoS$_2$.
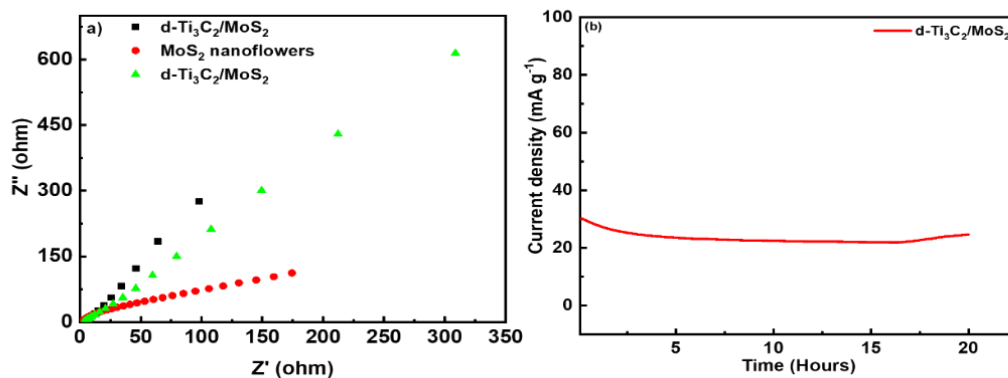
Figure 4. a) EIS of d-Ti$_3$C$_2$ MXene, MoS$_2$ nanoballs and d-Ti$_3$C$_2$/MoS$_2$ b) Chronoamperometry of d-Ti$_3$C$_2$/MoS$_2$

4. CONCLUSION

In our work, we have synthesized d-Ti$_3$C$_2$/MoS$_2$ nanocomposite by hydrothermal approach. This material was tested for HER and showed an excellent overpotential of 45 mV compared to d-Ti$_3$C$_2$ MXene (98 mV) and MoS$_2$ nanoballs (92 mV) using 2M KOH. This outstanding catalytic activity was attributed to the synergistic effect of both MXene and MoS$_2$ nanoballs, where MoS$_2$ prevents restacking of MXene and increase surface area by successful incorporation. The material showed outstanding stability for 20 h. These obtained results open an avenue to fabricate efficient and cost-effective electrodes by simple hydrothermal strategy for practical electrochemical water splitting.

REFERENCES

[1] K. Li, J. Xu, C. Chen, Z. Xie, D. Liu, D. Qu, H. Tang, Q. Wei, Q. Deng, J.J.J.o.C. Li, *J. Colloid Interface Sci*. 582, 591-597. **(2021)**

[2] Q. Xu, J. Zhang, H. Zhang, L. Zhang, L. Chen, Y. Hu, H. Jiang, C.J.E. Li, *Energy Environ. Sci.* 14, 5228-5259. **(2021)**.

[3] A.K. Ipadeola, A.K. Lebechi, L. Gaolatlhe, AB Haruna, M. Chitt, K. Eid, A.M. Abdullah, *KIJEC, Electrochem. Commun*. 136, 107207. **(2022)**

[4] W.-K. Chong, B.-J. Ng, L.-L. Tan, S.-P.J.E. *Chai, Fuels*, *Energy Fuels,* 36, 4250-4267. **(2022)**

[5] Y. Li, Z. Yin, M. Cui, X. Liu, J. Xiong, S. Chen, T.J.J.o.M.C.A. Ma, *J. Mater. Chem A*, 9, 2070-2092. **(2021)**

[6] Z. Zhu, J. Hao, H. Zhu, S. Sun, F. Duan, S. Lu, MJAFM Du, *Advance Fiber. Mater*, 3, 117-127. **(2021)**

[7] D.T. Tran, S. Prabhakaran, D.H. Kim, N. Hameed, H. Wang, N.H. Kim, JHJNE Lee, *Nano Energy*. 88, 106277. **(2021)**

[8] X. Ji, Y. Lin, J. Zeng, Z. Ren, Z. Lin, Y. Mu, Y. Qiu, J.J.N.c. Yu, *Nat. Commun,* 12, 1-13. **(2021)**

[9] Y. Guo, J. Tang, J. Henzie, B. Jiang, W. Xia, T. Chen, Y. Bando, Y.-M. Kang, M.S.A. Hossain, Y.J.A.n. Sugahara, *ACS Nano*. 14, 4141-4152. **(2020)**

[10] J. Zhou, J. Lin, H. Sims, C. Jiang, C. Cong, J.A. Brehm, Z. Zhang, L. Niu, Y. Chen, YJAM Zhou, *Adv. Mater.* 32, 1906536. **(2020)**

[11] T. Dong, X. Zhang, P. Wang, H.-S. Chen, *PJEA Yang, Electrochim. Acta*, 338, 135885. **(2020)**

[12] M. Nemiwal, T.C. Zhang, D.J.I.J.o.H.E. Kumar, *Int. J. Hydrog. Energy*. 46, 21401-21418. **(2021)**

[13] Y. Tang, C. Yang, X. Xu, Y. Kang, J. Henzie, W. Que, YJAEM Yamauchi, MXene *Nanoarchitectonics: Adv. Energy Mater*. 12, 2103867. **(2022)**

[14] J. Qiao, L. Kong, S. Xu, K. Lin, W. He, M. Ni, Q. Ruan, P. Zhang, Y. Liu, *WJESM Zhang, Energy Stor. Mater.* 43, 509-530. **(2021)**

[15] X. Zhang, X. Zhang, P.J.J.o.E.C. Yang, 895, 115510. **(2021)**

[16] S. Riyajuddin, K. Azmi, M. Pahuja, S. Kumar, T. Maruyama, C. Bera, K.J.A.n. Ghosh, *ACS Nano*. 15 5586-5599. (2021)

[17] M. Naguib, M.W. Barsoum, Y.J.A.M. Gogotsi, *Adv. Mater*. 33, 2103393. **(2021)**

[18] X. Jiang, A.V. Kuklin, A. Baev, Y. Ge, H. Ågren, H. Zhang, *PNJPR Prasad, Phys. Rep.* 848, 1-58. **(2020)**

[19] A. Bhat, S. Anwer, K.S. Bhat, M.I.H. Mohideen, K. Liao, A.J.n.D.M. Qurashi, 2D *Mater. Appl.* 5 1-21. **(2021)**

[20] J. Huang, Z. Li, Y. Mao, ZJNS Li, *Nano Select*. 2, 1480-1508. **(2021)**

[21] K. Ba, D. Pu, X. Yang, T. Ye, J. Chen, X. Wang, T. Xiao, T. Duan, Y. Sun, B.J.A.C.B.E. Ge, *Appl. Catal*. 317, 121755. **(2022)**

[22] H. Zhang, Z. Wang, Q. Zhang, F. Wang, Y.J.B. Liu, *Bioelectronics*, *Biosens. Bioelectron.* 124 184-190. **(2019)**

[23] Q. Kong, H. Zhang, Z. Yuan, J. Liu, L. Li, Y. Fan, G. Fan, BJASC Liu, *ACS Sustainable Chem. Eng.* 8 4755-4763. **(2020)**

[24] M. Alhabeb, K. Maleski, T. Mathis, A. Sarycheva, C. Hatter, S. Uzun, A. Levitt, Y. Gogotsi, Angew. *Chem. Int.* Ed. 57 5444-5448. **(2018)**